REPORT DOCUMENTATION PAGE		*Form Approved* *OMB No. 0704-0188*

maintaining the
data needed, and completing and reviewing this collection of information. Send comments regarding this burden estimate or any other aspect of this collection of information, including suggestions for reducing this burden to Department of Defense, Washington Headquarters Services, Directorate for Information Operations and Reports (0704-0188), 1215 Jefferson Davis Highway, Suite 1204, Arlington, VA 22202-4302. Respondents should be aware that notwithstanding any other provision of law, no person shall be subject to any penalty for failing to comply with a collection of information if it does not display a currently valid OMB control number. **PLEASE DO NOT RETURN YOUR FORM TO THE ABOVE ADDRESS.**

1. REPORT DATE *(DD-MM-YYYY)* 05-05-2000	2. REPORT TYPE Journal Article	3. DATES COVERED *(From - To)* 1 Oct 96 – 30 Sept 00
4. TITLE AND SUBTITLE 640x486 Long-Wavelength Two-Color GaAs/AlGaAs Quantum Well Infrared Photodetector (QWIP) Focal Plane Array Camera		5a. CONTRACT NUMBER
		5b. GRANT NUMBER
		5c. PROGRAM ELEMENT NUMBER 61102F
6. AUTHOR(S) Gunapala SD, Bandara SV, Singh A, Liu JK, Rafol SB, Luong EM, Mumolo JM, Tran NQ, Ting DZY, Vincent JD, Shott CA, Long J, LeVan PD		5d. PROJECT NUMBER 2305
		5e. TASK NUMBER TJ
		5f. WORK UNIT NUMBER 02
7. PERFORMING ORGANIZATION NAME(S) AND ADDRESS(ES) Air Force Research Laboratory 3550 Aberdeen Ave. SE Kirtland AFB, NM 87117-5776		8. PERFORMING ORGANIZATION REPORT NUMBER
9. SPONSORING / MONITORING AGENCY NAME(S) AND ADDRESS(ES)		10. SPONSOR/MONITOR'S ACRONYM(S)
		11. SPONSOR/MONITOR'S REPORT NUMBER(S)

12. DISTRIBUTION / AVAILABILITY STATEMENT
Approved for Public Release; Distribution is Unlimited.

20021212 120

13. SUPPLEMENTARY NOTES

14. ABSTRACT
We have designed and fabricated an optimized long-wavelength/very-long-wavelength two-color quantum well infrared photodetector (QWIP) device structure. The device structure was grown on a 3-in semi-insulating GaAs substrate by molecular beam epitaxy (MBE). The wafer was processed into several 640 x 486 format monolithically integrated 8-9 and 14-15 μm two-color (or dual wavelength) QWIP focal plane arrays (FPA's). These FPA's were then hybridized to 640 x 486 silicon CMOS readout multiplexers. A thinned (i.e., substrate removed) FPA hybrid was integrated into liquid helium cooled dewar for electrical and optical characterization and to demonstrate simultaneous two-color imagery. The 8-9 μm detectors in the FPA have shown background limited performance (BLIP) at 70 K operating temperature for 300 K background with $f/2$ cold stop. The 14-15 μm detectors of the FPA reach BLIP at 40 K operating temperature under the same background conditions. In this paper we discuss the performance of this long-wavelength dualband QWIP FPA in terms of quantum efficiency, detectivity, noise equivalent temperature difference (NE Δ T), uniformity, and operability.

15. SUBJECT TERMS
Dualband Infrared; Focal Plane Arrays; Gallium Arsenide; Large Format Imaging Arrays; Long-Wavelength Infrared; Quantum Well Infrared Photodetectors; Target Discrimination; Fabrication; Performance; Detectors

16. SECURITY CLASSIFICATION OF:			17. LIMITATION OF ABSTRACT	18. NUMBER OF PAGES	19a. NAME OF RESPONSIBLE PERSON David Cardimona
a. REPORT Unclassified	b. ABSTRACT Unclassified	c. THIS PAGE Unclassified	Unlimited	10	19b. TELEPHONE NUMBER *(include area code)* (505) 846-5807

i

Standard Form 298 (Rev. 8-98)
Prescribed by ANSI Std. 239.18

640 ×486 Long-Wavelength Two-Color GaAs/AlGaAs Quantum Well Infrared Photodetector (QWIP) Focal Plane Array Camera

Sarath D. Gunapala, Sumith V. Bandara, A. Singh, John K. Liu, Sir B. Rafol, E. M. Luong, Jason M. Mumolo, Nhan Q. Tran, David Z.-Y. Ting, *Member, IEEE,*, J. D. Vincent, Craig A. Shott, J. Long, and Paul D. LeVan

Abstract—We have designed and fabricated an optimized long-wavelength/very-long-wavelength two-color quantum well infrared photodetector (QWIP) device structure. The device structure was grown on a 3-in semi-insulating GaAs substrate by molecular beam epitaxy (MBE). The wafer was processed into several 640 × 486 format monolithically integrated 8–9 and 14–15 μm two-color (or dual wavelength) QWIP focal plane arrays (FPA's). These FPA's were then hybridized to 640 × 486 silicon CMOS readout multiplexers. A thinned (i.e., substrate removed) FPA hybrid was integrated into a liquid helium cooled dewar for electrical and optical characterization and to demonstrate simultaneous two-color imagery. The 8–9 μm detectors in the FPA have shown background limited performance (BLIP) at 70 K operating temperature for 300 K background with $f/2$ cold stop. The 14–15 μm detectors of the FPA reaches BLIP at 40 K operating temperature under the same background conditions. In this paper we discuss the performance of this long-wavelength dualband QWIP FPA in terms of quantum efficiency, detectivity, noise equivalent temperature difference (NEΔT), uniformity, and operability.

Index Terms—Dualband infrared, focal plane arrays, gallium arsenide, large format imaging arrays, long-wavelength infrared, quantum well infrared photodetectors, target discrimination.

I. INTRODUCTION

A GREAT number of infrared applications require the use of long-wavelength, dualband focal plane arrays (FPA's). For example, a two-color FPA camera would provide the absolute temperature of a target with unknown emissivity, which is extremely important in the process of identifying temperature difference between missile targets, warheads, and decoys. Dualband infrared FPA's can also play many important roles in Earth and planetary remote sensing, astronomy, etc. Furthermore, monolithically integrated dualband FPA's eliminate the need for beam splitters, filters, moving filter wheels, and rigorous optical alignment requirements imposed

on dualband systems based on separate FPA's or a broadband FPA. Two-color FPA's also reduce the mass, volume, and power requirements of dualband systems. Due to inherent properties such as narrow-band response, wavelength tailorability, and stability (i.e., low $1/f$ noise) associated with GaAs based QWIP's [1]–[6], it is an ideal candidate for large format long-wavelength multi-color FPA's. GaAs based quantum well infrared photodetectors (QWIP's) will also provide high uniformity, high operability (i.e., percentage of the number of pixels giving <100 mK noise equivalent temperature difference under the operation conditions described in this paper), and low cost as a result of mature GaAs growth and processing technology. In this paper, we discuss the first demonstration of a long- and very-long wavelength infrared (LWIR/VLWIR) imaging camera, based on a monolithically integrated 640 × 486 dualband QWIP FPA.

Until recently, the most developed and discussed two-color QWIP detector was the voltage tunable two stack QWIP. This device structure consists of two connected multi-quantum well (MQW) structures tuned to two different wavelength bands of interest. This device structure utilizes the advantage of electric field domains formation to select the response of one or the other detector [7], [8]. The major disadvantages of this type of two-color QWIP FPA are that the detector pixels need two different bias voltages to operate, and the long-wavelength sensitive segment of the device needs very high bias voltage (>8 V) to turn on the long-wavelength infrared (LWIR) detection. Another disadvantage is that the voltage tunable scheme will not provide simultaneous data from both wavelength bands.

II. DEVICE STRUCTURE

The LWIR/VLWIR dualband QWIP device structure described in this section can be processed into either simultaneously readable dualband FPA's with triple contacts to access the CMOS readout multiplexer [9], or interlace readable dualband FPA's (i.e., odd rows for one color and the even rows for the other color). The first approach requires a special dualband readout multiplexer containing two readout cells for each detector unit cell (contains two vertically integrated detectors), while the second approach needs only an existing single color CMOS readout multiplexer. The advantages of second scheme are that it provides simultaneous data acquisition and allows the use of currently available single color CMOS readout multiplexers. However, the disadvantage is that it does not
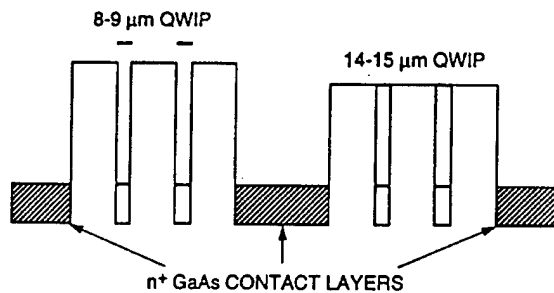
Fig. 1. Conduction band energy diagram of the long-wavelength and very long-wavelength two-color infrared detector. The long-wavelength (8–9 μm) sensitive MQW stack utilizes the bound-to-continuum intersubband absorption. The very long-wavelength (14–15 μm) sensitive MQW stack utilizes the bound-to-quasibound intersubband absorption.
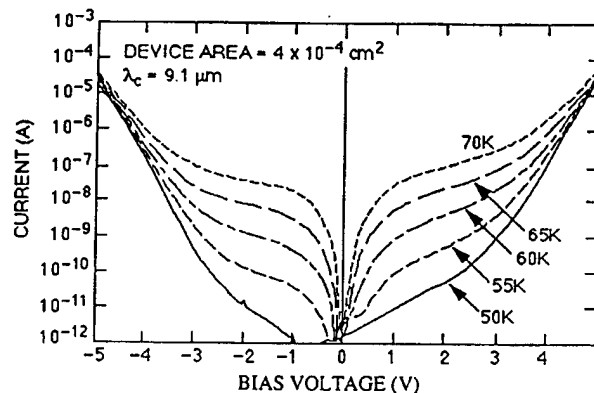

Fig. 2. Dark current versus voltage curves of a LWIR detector at various temperatures. The device area is 4×10^{-4} cm^2.
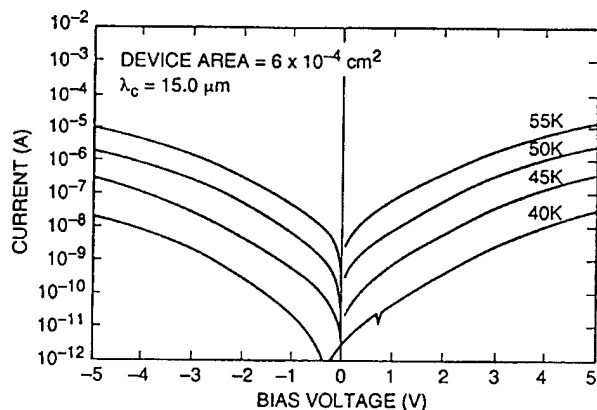

Fig. 3. Dark current versus voltage curves of a VLWIR detector at various temperatures. The device area is 4×10^{-4} cm^2.

provide a full fill factor for both wavelength bands. This problem can be eliminated by fabricating $(n + 1)$ terminals (e.g., three terminals for dualband) per pixel and hybridizing with a multicolor readout having n readout cells per detector pitch, where n is the number of bands.

The device structure consists of a 30 period stack of VLWIR QWIP structure, and a 18 periods stack of LWIR QWIP structure, separated by a heavily doped 0.5 μm thick intermediate GaAs contact layer (see Fig. 1). The first stack (VLWIR) consists of 30 periods of a 500 Å Al$_x$Ga$_{1-x}$As barrier and a 60 Å GaAs well. Since the dark current of this device structure is dominated by the longer wavelength portion of the device structure, the VLWIR QWIP structure has been designed to have a bound-to-quasibound intersubband absorption peak at 14.5 μm. The second stack (LWIR) consists of 18 periods of a 500 Å Al$_x$Ga$_{1-x}$As barrier and a narrow 40 Å GaAs well. This LWIR QWIP structure has been designed to have a bound-to-continuum intersubband absorption peak at 8.5 μm, because the photocurrent and dark current of the LWIR device structure is relatively small compared to the VLWIR portion of the device structure. This whole dualband QWIP structure is then sandwiched between 0.5 μm GaAs top and bottom contact layers doped with $n = 5 \times 10^{17}$ cm^{-3}, and was grown on a semi-insulating GaAs substrate by MBE. A 300 Å Al$_{0.3}$Ga$_{0.7}$As stop-etch layer and a 1.0 μm thick GaAs cap layer were then grown in situ on top of the device structure. GaAs wells of the LWIR and VLWIR stacks were doped with $n = 6 \times 10^{17}$ and 2.5×10^{17} cm^{-3}, respectively. All contact layers were doped to $n = 5 \times 10^{17}$ cm^{-3}. The GaAs well doping density of the LWIR stack was intentionally increased by a factor of two to compensate for the reduced number of quantum wells in the LWIR stack. It is worth noting that, the total (dark current + photo current) current of each stack can be independently controlled by carefully designing the position of the upper state, well doping densities, and the number of periods in each MQW stack. All of these features were utilized to obtain approximately equal total currents from each MQW stack. Fig. 1 shows the conduction band energy diagram of this dualband QWIP device structure [10], [11].

Using both selective and nonselective dry etching, this MBE grown device structure was processed into 200 $\times$ 200 μm^2 test devices. Au/Ge ohmic contacts were evaporated onto the top,

middle, and bottom contact layers. These test detectors were back illuminated through a 45° polished facet as described elsewhere [5]. The simultaneously measured dark current-voltage curves and responsivity spectra of these vertically integrated dualband QWIP's are shown in Figs. 2–4. The low temperature dark current curves showed a pronounced zero bias offset. The offsets switched polarity when the direction of the voltage scans were reversed. Also, the offsets were found to depend on the delay in applied bias, indicative of an RC time constant effect (see [12] for a detail discussion). The responsivity of the LWIR detectors peaks at 8.4 μm and the peak responsivity (R_p) of the detector is 509 mA/W at bias $V_B = -2$ V. The spectral width and the cutoff wavelength of the LWIR detectors are $\Delta\lambda/\lambda = 16\%$ and $\lambda_c = 9.1$ μm, respectively. The responsivity of the VLWIR detectors peaks at 14.4 μm and the peak responsivity (R_p) of the detector is 382 mA/W at bias $V_B = -2.0$ V. The spectral width and the cutoff wavelength of the VLWIR detector are $\Delta\lambda/\lambda = 10\%$ and $\lambda_c = 15$ μm, respectively. The measured absolute peak responsivity of both LWIR and VLWIR detectors is small, up to about $V_B = -0.5$ V. Beyond that, it increases almost linearly with bias in both LWIR and VLWIR detectors reaching $R_P = 0.3$ (at $V_B = -2$ V) and 1 A/W (at $V_B = -3$ V), respectively. This behavior
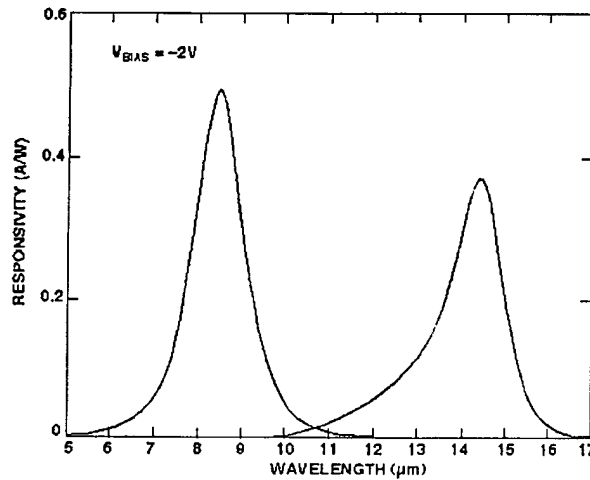
Fig. 4. Simultaneously measured responsivity spectrum of vertically integrated LWIR and VLWIR dualband QWIP detector (45° illumination).

Fig. 5. Calculated dark current limited (zero background) peak detectivity D^* of LWIR detectors as a function of bias voltage at seven different operating temperatures.

Fig. 6. Calculated dark current limited (zero background) peak detectivity D^* of a VLWIR detector as a function of bias voltage at seven different operating temperatures.

of responsivity versus bias is typical for bound-to-continuum and bound-to-quasibound QWIP's in LWIR and VLWIR bands. The peak absorption quantum efficiencies of the LWIR and the VLWIR detectors operating at a bias of $V_B = -2$ V are 6.4% and 11.6%, respectively.

The photoconductive gain g was experimentally determined using $g = i_n^2/4el_DB$, where B is the measurement bandwidth, and i_n is the current noise, which was measured using a spectrum analyzer [13]. The photoconductive gains of the LWIR and VLWIR MQW stacks reached 0.98 and 0.27, respectively, at $V_B = -2$ V. These photoconductive gains show that the VLWIR gain is almost a factor of four lower than that of the LWIR. This is attributed to the lower number of periods (i.e., approximately a factor of two) and the bound-to-continuum device structure (as shown in Fig. 2) of LWIR MQW stack as compared to the VLWIR MQW structure (i.e., bound-to-quasibound). It has been shown previously that bound-to-quasibound QWIP's have much lower photoconductive gain and responsivity compared to the bound-to-continuum QWIP's (see [5] for a detail discussion). The peak detectivity is defined as $D_p^* = R_p\sqrt{AB}/i_n$, where R_p is the peak responsivity, and A is the area of the detector. The areas of the LWIR and VLWIR detectors are 4×10^{-4} and 6×10^{-4} cm^2 respectively. The zero background peak detectivities of both LWIR and VLWIR detectors were estimated at different operating temperatures and bias voltages using experimentally measured noise currents, and the results are shown in Figs. 5 and 6. Basically, the zero background detectivity is the dark current limited detectivity. Based on single element test detector data, the LWIR detectors show background limited performance (BLIP) at bias $V_B = -2$ V and temperature $T = 72$ K for a 300 K background with $f/2$ cold stop. The VLWIR detectors reached BLIP under the same operating conditions at 45 K operating temperature.

III. FOCAL PLANE ARRAYS

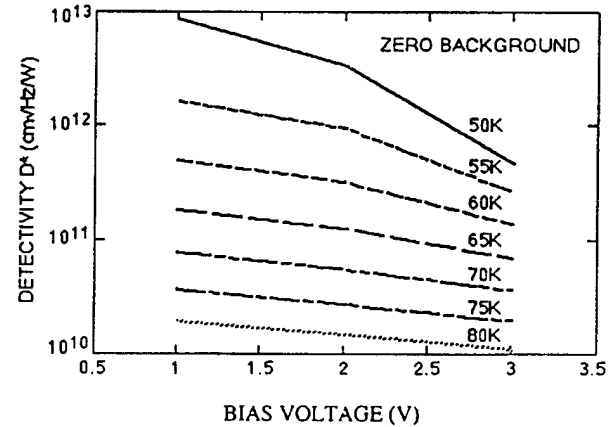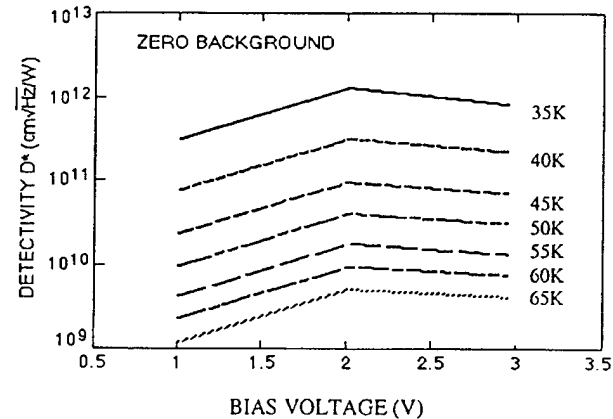It is well known that GaAs/AlGaAs based n-type QWIP's do not absorb infrared radiation incident normal to the surface.

Thus, researchers have invented various light coupling schemes such as two-dimensional (2-D) periodic gratings [14], random reflectors [15], corrugated reflectors [16], lattice mismatch strain material systems, and p-type materials [17]. Many of our previous FPA's utilized random reflectors for efficient light coupling. Although random reflectors have achieved relatively high quantum efficiencies with large test device structures, it is not possible to achieve similar high quantum efficiencies with random reflectors on small FPA pixels due to the reduced width-to-height aspect ratios. In addition, it is difficult to fabricate random reflectors for shorter wavelength detectors compared to very long-wavelength detectors (i.e., 15 μm) due to the fact that feature sizes of random reflectors are linearly proportional to the peak wavelength of the detectors. For example, the minimum feature size of random reflectors of 15 and 9 μm cutoff FPA's were 1.25 and 0.6 μm, respectively. It is difficult to fabricate submicron features by contact photolithography. As a result, the random reflectors of the 9 μm cutoff FPA were less sharp and had fewer scattering centers compared to the random reflectors of the 15 μm cutoff
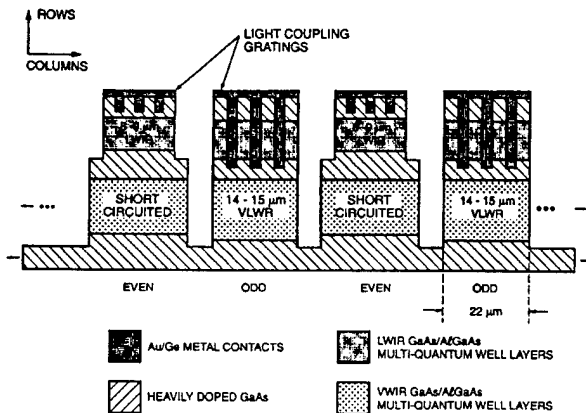
Fig. 7. Schematic side view of the interlace dualband FPA. The VLWIR detector pixels in even rows were short circuited at the row-ends. The LWIR detector pixels in odd rows were short circuited by fabricating VLWIR light coupling grating structure through the LWIR portion of detector pixels.

QWIP FPA. Thus, 2-D periodic grating structures were used for efficient light coupling for dualband QWIP's. As we have discussed before [5], two passes of infrared radiation can be coupled to the QWIP detector structure by incorporating a 2-D periodic grating surface [14] on top of the detectors.

Two distinct 2-D periodic grating structures were designed to independently couple the 8–9 and 14–15 μm radiation into the detector pixels of the even and odd rows of the FPA's. The top 0.7 μm thick GaAs cap layer was used to fabricate the light coupling 2-D periodic grating for 8–9 μm detector pixels. As shown in Fig. 7, the light coupling for 2-D periodic gratings of the 14–15 μm detector pixels were fabricated through the photosensitive LWIR MQW layers. This grating scheme short circuited all 8–9 μm sensitive detectors in all the odd rows of the FPA's. Thus, the total thickness of 8–9 μm detector is limited by the grating layer thickness of the VLWIR detector. This 2-D periodic grating structure is fabricated on the detectors by using standard photolithography and SF$_6$:BCl$_3$ selective dry etching.

After the 2-D grating array (calculations of the 2-D grating parameters and light coupling experiments were discussed extensively in [14]) was defined by photolithography and dry etching, the LWIR detector pixels of the 640 × 486 FPA's were fabricated by dry etching through the photosensitive GaAs/Al$_x$Ga$_{1-x}$As MQW layers into the 0.5 μm thick doped GaAs intermediate contact layer. All VLWIR pixels in the even rows of FPA's were short circuited. The VLWIR detector pixels of the FPA's were fabricated by dry etching both MQW stacks into the 0.5 μm thick heavily doped GaAs bottom contact layer. The pitch of the FPA is 25 μm, and the actual VLWIR and LWIR pixel sizes are 23 × 23 and 22 × 23 μm^2, respectively. The 2-D grating reflectors on top of the detectors were then covered with Au/Ge and Au for Ohmic contact and reflection. Twelve FPA's were processed on a 3-in GaAs wafer. Indium bumps were then evaporated on top of the detectors for silicon readout circuit (ROC) hybridization. Several dualband FPA's were chosen and hybridized (via an indium bump-bonding process) to a 640 × 486 CMOS multiplexer (Amber AE-181).

Gaps between the FPA detectors and the readout multiplexer were backfilled with epoxy. This epoxy backfilling provides the necessary mechanical strength to the hybridized FPA's prior to the thinning process. Substrate thinning (or substrate removal) is very important for the success of cryogenic FPA hybrids. During the first step of the thinning process, an approximately 500 μm thick GaAs layer was removed using abrasive polishing or diamond turning. Then bromine-methanol chemical polishing was used to remove another approximately 100 μm thick GaAs layer. This step is very important because it removes all scratch marks left on the substrate due to abrasive polishing. Otherwise, these scratch marks will be enhanced and propagated into the final step via preferential etching. Then, wet chemical etchant was used to reduce the substrate thickness to several microns and SF$_6$:BCl$_3$ selective dry etching was used as the final etch. This final etching completely removed the remaining GaAs substrate. At this point the remaining GaAs/AlGaAs material contains only the QWIP pixels and a very thin membrane ($\sim$ 1000 Å). The thermal mass of this membrane is insignificant compared to the rest of the hybrid. This allows it to adapt to the thermal expansion and contraction coefficients of the silicon readout multiplexer, completely eliminating the thermal mismatch between the silicon based readout and the GaAs based detector array. The procedure basically enables QWIP FPA's to go through an unlimited number of temperature cycling without any delamination. Furthermore, this substrate removal process provides two additional advantages for QWIP FPAs: the complete elimination of pixel-to-pixel optical cross-talk, and a significant enhancement in optical coupling of infrared radiation into QWIP pixels. In the case of 2-D periodic grating light coupling, this thinning provides a factor of two enhancement in light coupling due to the total internal reflection of the diffracted light with in the same pixel (see [5] for a detail discussion in light coupling techniques).

One selected dualband FPA hybrid was mounted onto the cold finger of a liquid helium cooled laboratory test dewar and biased at $V_B = -2$ V. This selected FPA was tested at temperature 40 K. At temperatures below 70 K, the signal-to-noise ratio of the LWIR detector pixels is limited by array nonuniformity, readout noise, and photo current noise (for $f/2$ cold stop). At temperatures above 70 K, temporal noise due to the QWIP's higher dark current becomes the limitation. As mentioned earlier, this higher dark current is due to thermionic emission and thus causes the charge storage capacitors of the readout circuitry to saturate. At temperatures below 40 K, the signal-to-noise ratio of VLWIR detector pixels is limited by array nonuniformity, readout noise, and photo current noise. Since the QWIP is a high impedance device, it yields a very high charge injection coupling efficiency into the integration capacitor of the multiplexer. The differential resistances R_{Det} of both LWIR and VLWIR pixels are 2.0×10^{12} and 7.0×10^{11} Ω, respectively, at −2 V bias, 40 K temperature, and $f/2$ field of view with 300 K background. The experimentally measured detector capacitance C_{Det} at temperature $T = 40$ K is 3.0×10^{-14} F. The input impedance and the capacitance of the input FET which is in parallel with the detector are 5.8×10^9 Ω and 2×10^{-14} F, respectively. Therefore, the total input impedance and capacitance of the input circuit are
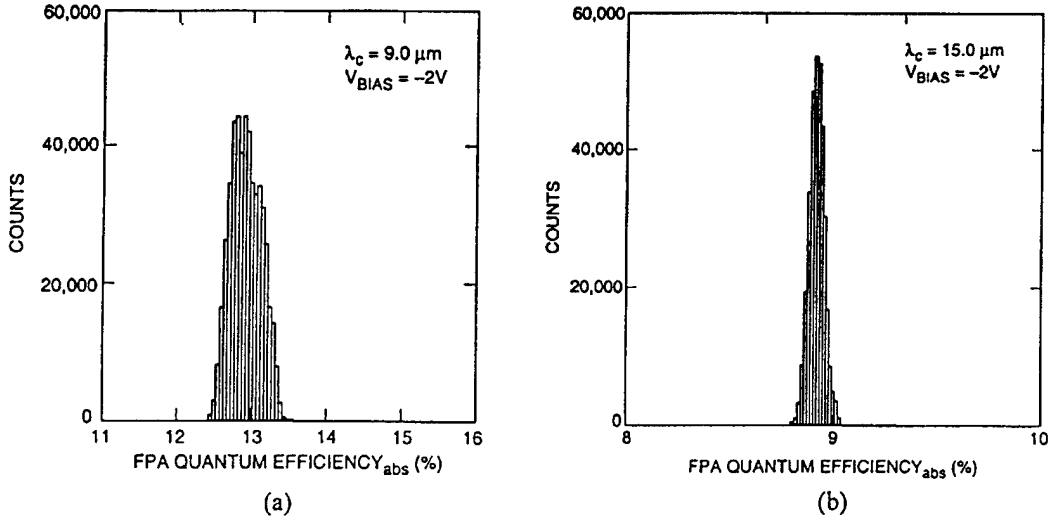
Fig. 8. (a) Uncorrected quantum efficiency histogram of 8–9 μm detector pixels of the 640 × 486 dualband FPA. The mean quantum efficiency is 12.9%. The nonuniformity (i.e., sigma/mean) is 2%. (b) Uncorrected quantum efficiency histogram of 14–15 μm detector pixels of the 640 × 486 dualband FPA. The mean quantum efficiency is 8.9%. The nonuniformity is 1%.

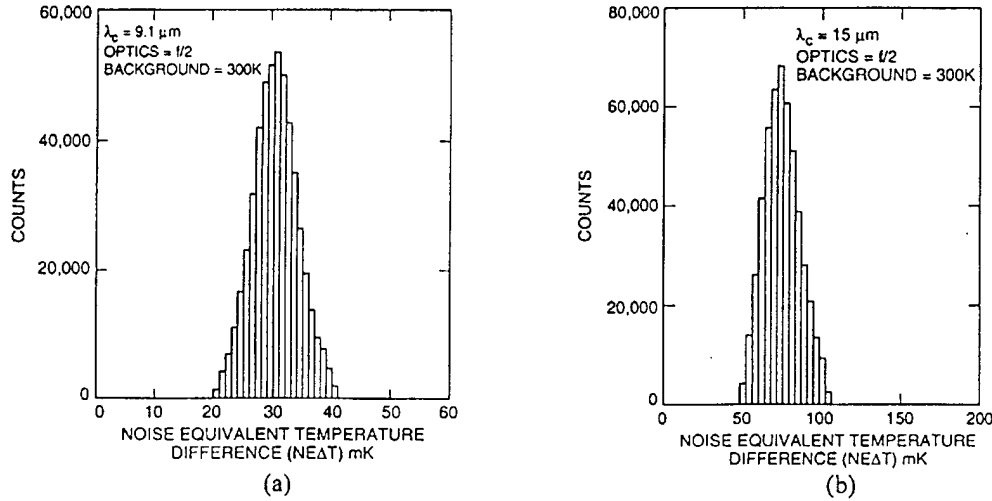Fig. 9. (a) Uncorrected noise equivalent temperature difference (NEΔT) histogram of 8–9 μm detector pixels of the 640 × 486 dualband FPA. The mean NEΔT is 29 mK. (b) Uncorrected NEΔT histogram of 14–15 μm detector pixels of the 640 × 486 dualband FPA. The mean NEΔT is 74 mK.

5.8 × 10^9 Ω and 5 × 10^{-14} F, respectively. Thus, the RC time constant of the input circuit is 290 μs. This basically sets the lower limit for the integration time. The integration time used during data acquisition is 3 msec. The detector dark currents at $T = 40$ K of LWIR and VLWIR detectors are 2.6 × 10^{-15} and 2.5 × 10^{-12} A, respectively. Charge injection efficiency into the CMOS readout multiplexer was calculated as described in [2]. The calculated charge injection efficiency exceeds 90% at a 30 Hz frame rate. The FPA was back-illuminated through the flat thinned substrate membrane (thickness ≈1000 Å). This FPA gave excellent images with 99.7% of the LWIR pixels and 98% of VLWIR pixels operable, demonstrating the high yield of GaAs technology. Here we define operability as the percentage of pixels having noise equivalent differential temperature less than 100 mK at a 300 K blackbody.

IV. RESULTS AND DISCUSSION

One dualband FPA was tested at a background temperature of 300 K, with $f/2$ cold stop, and at 30 Hz frame rate. Figs. 8(a) and (b) show the measured quantum efficiency of the FPA at an operating temperature of $T = 40$ K and bias $V_B = -2$ V. The mean value of the long-wavelength FPA net absorption quantum efficiency is 12.9% (see Fig. 8). This measured value is the integrated FPA net absorption quantum efficiency and is not corrected for the 30% substrate reflection loss and 85% FPA fill factor. This mean quantum efficiency is a factor of 2.1 higher than the 45° double pass quantum efficiency. This agrees well with typical 2-D periodic grating light coupling efficiencies reported in other experiments. The uncorrected nonuniformity (i.e., sigma/mean) of the quantum efficiency histogram is 2%.
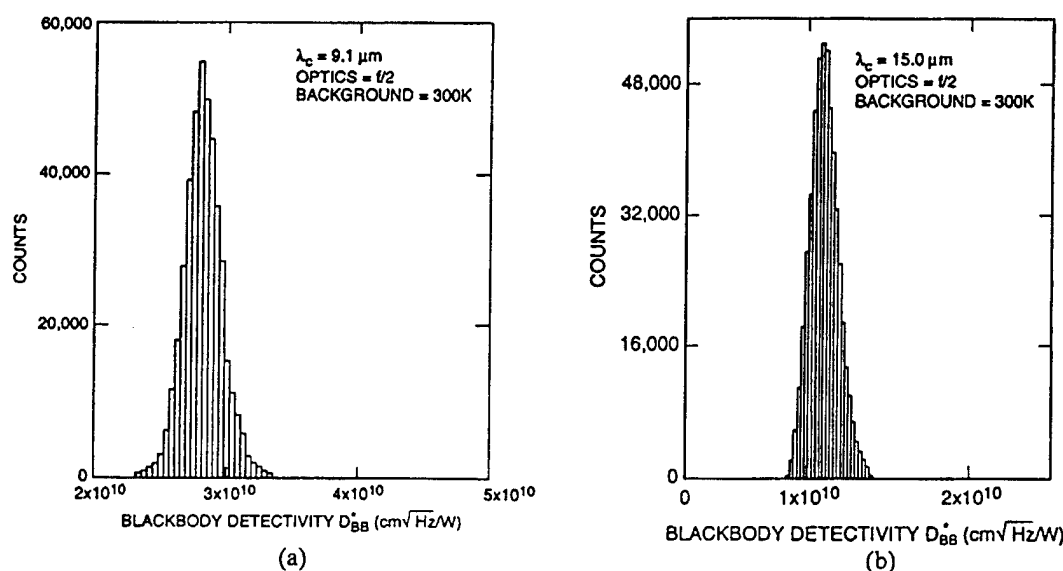
(a)

(b)

Fig. 10. (a) Uncorrected 300 K blackbody detectivity D_{BB}^* histogram of 8–9 μm detector pixels of the 640 × 486 dualband FPA. The mean blackbody detectivity D_{BB}^* is 2.9 × 10^{10} cm$\sqrt{\text{Hz}}$/W. (b) Uncorrected 300 K blackbody detectivity D_{BB}^* histogram of 14–15 μm detector pixels of the 640 × 486 dualband FPA. The mean blackbody detectivity D_{BB}^* is 1.1 × 10^{10} cm$\sqrt{\text{Hz}}$/W.

The mean quantum efficiency of 14–15 μm detector pixels in the FPA is 8.9%, and the uncorrected quantum efficiency nonuniformity is about 1%. This mean FPA quantum efficiency value is a factor of 1.3 lower than the 45° test detector quantum efficiency. This shows that the 2-D periodic grating light coupling is very effective in the LWIR region compared to VLWIR region.

As expected (due to BLIP), the estimated and experimentally obtained NEΔT values of the LWIR detectors do not change significantly at temperatures below 65 K. The estimated NEΔT of LWIR and VLWIR detectors at 40 K are 36 and 44 mK, respectively [see Figs. 9(a) and (b))]. These estimated NEΔT values based on the test detector data agree reasonably well with the experimentally obtained values. The experimental NEΔT value is lower than the estimated NEΔT value of 36 mK. This improvement is attributed to the 2-D periodic grating light coupling efficiency. On the other hand the experimental VLWIR NEΔT value is higher than the estimated NEΔT value of 44 mK. This degradation in performance could be attributed to the inefficient light coupling at 14–15 μm region, readout noise, and the noise of the proximity electronics. At 40 K the performance of both LWIR and VLWIR detector pixels of this dualband FPA is limited by the photo current noise and readout noise.

The uncorrected FPA blackbody detectivity histograms of both LWIR and VLWIR detector pixels are shown in Figs. 10(a) and (b). This detectivity data was acquired at 300 K background with $f/2$ cold stop. The mean blackbody detectivity D_{BB}^* values of the LWIR and VLWIR pixels are 2.9 × 10^{10} and 1.1 × 10^{10} cm$\sqrt{\text{Hz}}$/W, respectively. This shows that the 8–9 μm part of this imaging system is 35% BLIP at 300 K background with $f/2$ cold stop. The 14–15 μm part of the imaging system reachs 15% BLIP at the same operating condition. However, according to theoretical estimates based on single element test detector data, both the LWIR and VLWIR detector pixels should have reached 100% BLIP at 40 K operating
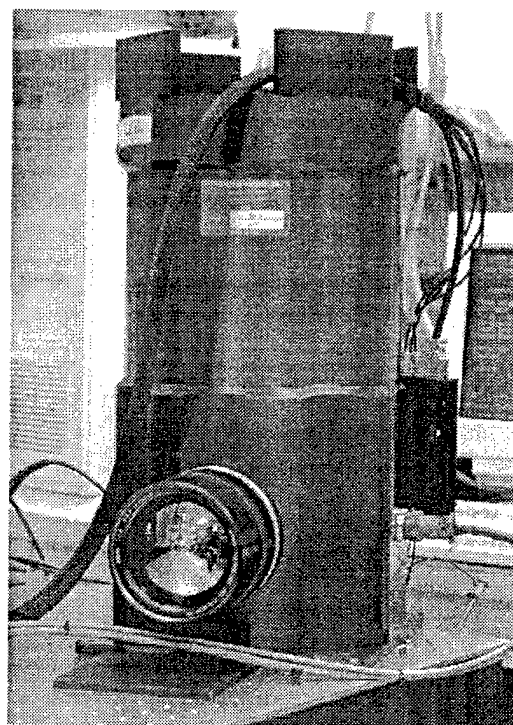

Fig. 11. Picture of the 8–9 and 14–15 μm dualband imaging camera.

temperature. This clearly shows that the performance of this dualband imaging system is limited by the noise of the readout multiplexer and dewar proximity electronics.

A dualband FPA hybrid was mounted onto the cold finger of a liquid helium cooled laboratory dewar, to demonstrate simulta-
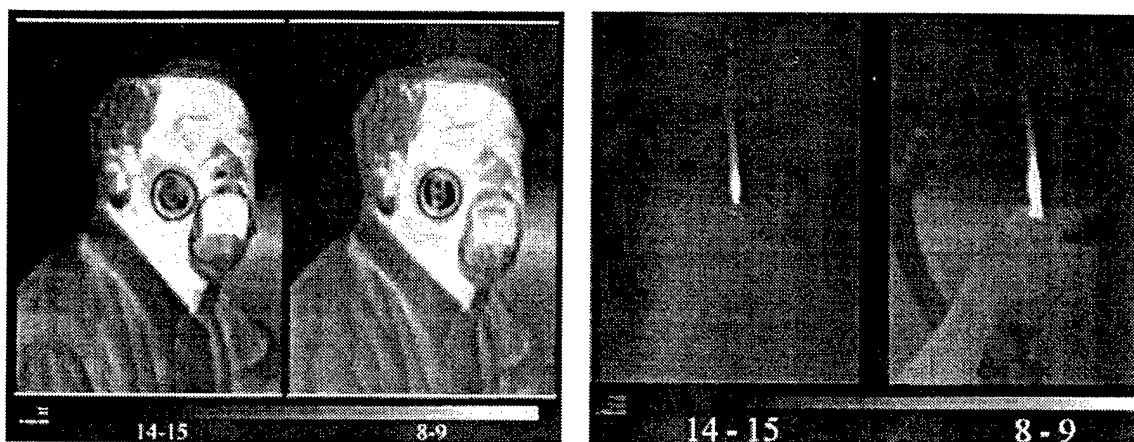
Fig. 12.   Both pictures show (Flame—simultaneously acquired) two-color images with the 640 × 486 two-color QWIP camera. Image on the left is from 14–15 μm infrared and the image on the right is from 8–9 μm infrared. Pixel pitch of the FPA is 25 μm. The 14–15 μm image is less sharp due to the diffraction limited spot size being larger than the pixel pitch of the FPA.

(a)   (b)
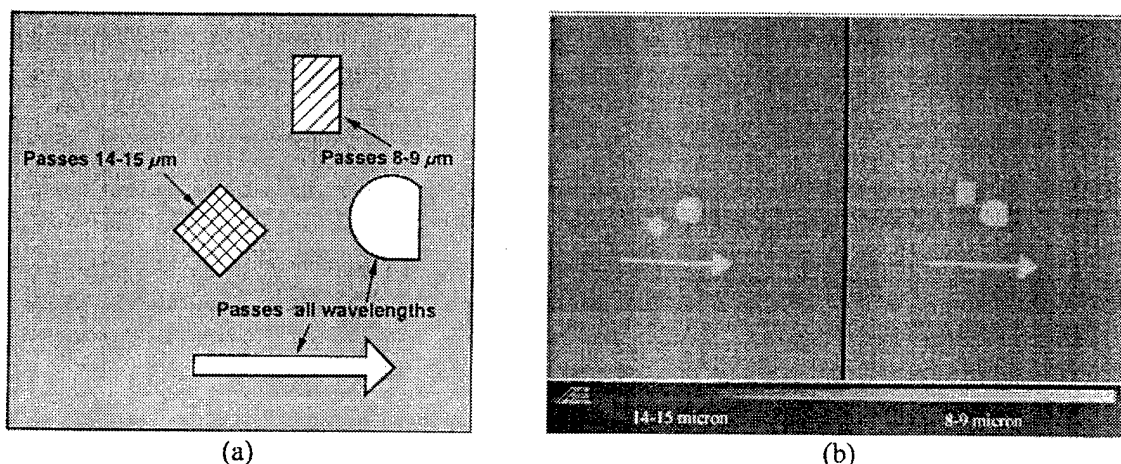
Fig. 13.   (a) Piece of cardboard with some openings. The arrow and the semicircle are open, and transmit all wavelengths. The diamond shape opening is covered with a 10 μm highpass filter and the rectangle shape is covered with a 10 μm lowpass filter. (b) Simultaneously acquired image of the object described in (a). This clearly verifies the 8–9 and 14–15 μm two-color operation of this QWIP camera.

neous dualband imagery at 8.5 and 14.5 μm (shown in Fig. 11). The camera is equipped with a 100 mm focal length $f/2$ germanium lens designed to be transparent in the 8–15 μm wavelength range, for compatibility with the 8–9 and 14–15 μm dualband operation. Due to transmission properties of germanium, the 14–15 μm band has only 30% transmission. This poor optical transmission has clearly affected the VLWIR performance and image quality. Pixels having NEΔT > 100 mK are counted as dead pixels. Thus, the operability of 8–9 μm detector pixels is 99.7% and the operability of 14–15 μm detector pixels is 98%. However, the actual number of dead pixels (i.e., no photo response) is less than 50, thereby making pixel replacement software unnecessary. It should be noted that this initial FPA is far from optimum and does not represent the best obtainable nonuniformity and operability.

Video images were taken at a frame rate of 30 Hz, at temperatures as high as $T = 74$ K, using a ROC capacitor having a charge capacity of 9 × 10^6 electrons (the maximum

number of photoelectrons and dark electrons that can be counted in the time taken to read each detector pixel). Fig. 12 shows simultaneously acquired 8–9 and 14–15 micron images using this two-color (LWIR and VLWIR) imaging camera. Fig. 13(a) shows a drawing of the filter pattern used to test the operating wavelengths of the two-color camera. The arrow and the semi-circle are open, and transmit all wavelengths. The diamond shape opening is covered with a 10 μm highpass filter, and the rectangle shape opening is covered with a 10 μm lowpass filter. Fig. 13(b) shows a simultaneously acquired image of the object described in the Fig. 13(a). This clearly demonstrates the 8–9 and 14–15 μm two-color operation of this dualband QWIP camera. The readout multiplexer used was a photovoltaic InSb multiplexer which was not optimized to supply the proper bias and impedance levels required by photoconductive QWIP's. Implementation of these improvements should significantly enhance the QWIP FPA operating temperature (i.e., 80 K for 9 μm).

In summary, we have demonstrated the first 8–9 and 14–15 μm two-color imaging camera based on a 640 × 486 dualband QWIP FPA. NEΔT of 36 and 44 mK have been achieved at LWIR and VLWIR spectral bands, respectively. Excellent simultaneous imagery at LWIR and VLWIR spectral bands have been demonstrated at 30 Hz.

ACKNOWLEDGMENT

REFERENCES

[1] S. D. Gunapala *et al.*, "Long-wavelength 640 × 484 GaAs/Al$_x$Ga$_{1-x}$As quantum well infrared photodetector focal plane array camera," *Proc. SPIE*, vol. 3061, pp. 722–727, 1997.

[2] S. D. Gunapala *et al.*, "9 μm cutoff 256 × 256 GaAs/Al$_x$Ga$_{1-x}$As quantum well infrared photodetector hand-held camera," *IEEE Trans. Electron Devices*, vol. 44, pp. 51–57, 1997.

[3] J. Y. Andersson *et al.*, "320 × 240 pixels quantum well infrared photodetector (QWIP) array for thermal imaging: Fabrication and evaluation," *SPIE*, vol. 3061, pp. 740–748, 1997.

[4] W. A. Beck *et al.*, presented at the 2nd Int. Symp. 2–20 μm Wavelength Infrared Detectors and Arrays: Physics and Applications, Miami Beach, FL, Oct. 10–12, 1994.

[5] S. D. Gunapala and S. V. Bandara, "Quantum well infrared photodetector (QWIP) focal plane arrays," in *Semiconductors and Semimetals*. New York: Academic , 1999, vol. 62, pp. 197–282.

[6] M. Sundaram *et al.*, "Two-color MW/LW QWIP FPA and commercial one-color LW QWIP FPA," in *Proc. 1st Int. Symp. Advanced Luminescent Materials and Quantum Confinement, 196th Meeting Electrochem. Soc.*, vol. PV 99-22, 1999, pp. 459–473.

[7] I. Grave, A. Shakouri, N. Kuze, and A. Yariv, "Control of electric field domain formation in multiquantum well structures," *Appl. Phys. Lett.*, vol. 63, pp. 1101–1103, 1993.

[8] T. Mei, G. Karunasiri, and S. J. Chua, "Two-color infrared detection using intersubband transitions in multiple step quantum wells with superlattice barriers," *Appl. Phys. Lett.*, vol. 71, pp. 2017–2019, 1997.

[9] S. D. Gunapala *et al.*, "Quantum well infrared photodetectors for low-background applications," *Proc. SPIE*, vol. 3379, pp. 225–234, 1998.

[10] Ph. Bois *et al.*, "Optimized multiquantum well infrared detectors," *Proc. SPIE*, vol. 2552, pp. 755–766, 1995.

[11] M. Z. Tidrow, J. C. Chiang, S. S. Li, and K. Bacher, "A high strain two-stack two-color quantum well infrared photodetector," *Appl. Phys. Lett.*, vol. 70, pp. 859–861, 1997.

[12] A. Singh and D. A. Cardimona, "Zero bias offsets in the low temperature dark current characteristics of QWIPs," *Opt. Eng.*, vol. 38, pp. 1424–1432, 1999.

[13] G. Hasnain, B. F. Levine, S. Gunapala, and N. Chand, "Large photoconductive gain in quantum well infrared photodetectors," *Appl. Phys. Lett.*, vol. 57, pp. 608–610, 1990.

[14] J. Y. Andersson, L. Lundqvist, and Z. F. Paska, "Quantum efficiency enhancement of AlGaAs/GaAs quantum well infrared detectors using a waveguide with a grating coupler," *Appl. Phys. Lett.*, vol. 58, pp. 2264–2266, 1991.

[15] G. Sarusi, B. F. Levine, S. J. Pearton, K. M. S. V. Bandara, and R. E. Leibenguth, "Improved performance of quantum well infrared photodetectors using random scattering optical coupling," *Appl. Phys. Lett.*, vol. 64, pp. 960–962, 1994.

[16] K. K. Choi *et al.*, "Corrugated QWIP array fabrication and characterization," *Proc. SPIE*, vol. 3287, pp. 118–127, 1998.

[17] S. S. Li and Y. H. Wang, "Novel grating coupled and normal incidence III-V quantum well infrared photodetectors with background limited performance at 77K," in *Quantum Well Intersubband Transition Physics and Devices, NATO ASI Series*. Boston, MA: Kluwer, 1994, vol. 270, pp. 29–42.

Sarath D. Gunapala received the B.S. degree in physics from the University of Colombo, Sri Lanka, in 1980, M.S. and the Ph.D. in physics from the University of Pittsburgh, Pittsburgh, PA, in 1986.

He studied properties of thin films as a Research Associate at the Bell Communications Research from 1986 to 1988. From 1988 to 1991, he was a Post-doctoral Member of Technical Staff at AT&T Bell Laboratories, Murray Hill, NJ, where he participated in the development of quantum well infrared photodetectors for infrared imaging. He joined NASA's Jet Propulsion Laboratory, California Institute of Technology, Pasadena, in 1992. There, he leads the QWIP research group. He has authored over 100 publications, including several book chapters on quantum well infrared photodetectors.

Sumith Bandara received the Ph.D. degree from the University of Pittsburgh, Pittsburgh, PA, in 1989.

He is a Senior Member of Engineering Staff at Jet Propulsion Laboratory (JPL), California Institute of Technology, Pasadena, and has over ten years of experience in QWIP research. Prior to joining JPL, he was with Bell Laboratories, Murray Hill, NJ, and at the University of Pittsburgh. His work involved new types of QWIP device design, theoretical modeling, fabrication, optical coupling and performance analysis. He has designed several QWIP focal plane arrays including broad-band 10–16 μm 640 × 486 format FPA. He has authored and co-authored over 75 technical publications including an extensive review of QWIP's.

A. Singh received the B.E. (hons.) degree from the University of Madras, India, the M.S. degree from the Indian Institute of Technology, Madras, India, and the Ph.D. degree from the University of Rhode Island, Kingston, all in electrical engineering.

She was a National Research Council Post-Doctoral Fellow at the Air Force Phillips Laboratory, Kirtland AFB, NM, where she initially began investigating the low temperature physics of QWIP's. She is currently a Research Assistant Professor at the University of New Mexico, Albuquerque, and an IPA at the Air Force Research Laboratory, where she continues to pursue her work in low background-low temperature QWIP's, long-wave and multicolor infrared detectors, and smart sensors.

John K. Liu received the B.S. degree in engineering science/bioengineering from the University of California, San Diego, in 1984, and the M.S.E.E. degree from California State University, Los Angeles, in 1986.

From 1985 to 1989, he worked at the Jet Propulsion Laboratory (JPL), California Institute of Technology, Pasadena, on solar cell and III-V MBE growth. From 1989 to 1991, he was with TRW, Redondo Beach, CA, where he worked on III-V thin film growth using MBE for MMIC applications. Since 1991, he has been working on the development of QWIP IR camera at JPL. His current interest is on QWIP FPA fabrications and characterizations.

Sir B. Rafol received the B.E.E.T. degree from DeVry Institute of Technology in Chicago, IL, in 1976, the M.A. degree in physics degree from Kent State University, Kent, OH, in 1982, and the Ph.D. degree in physics from University of Illinois, Chicago, in 1991.

He joined USRobotics, Mount Prospect, IL, in 1995 and Rockwell, Woods Dale, IL, in 1997, where he worked on telecommunication system. In 1998, he joined Jet Propulsion Laboratory, California Institute of Technology, Pasadena, where he has been working on characterization of QWIP focal plane array and detector development. His research interest is on magnetotransport properties of low dimensional quantum systems and quantum detectors.

David Z.-Y. Ting (M'99) was born in Taipei, Taiwan, R. O. C., in 1957. He received the B.S. degree with honors in physics from the California Institute of Technology (Caltech), Pasadena, in 1980, and the M.S. and Ph.D. degrees in physics from the University of Illinois at Urbana-Champaign in 1981 and 1986, respectively.

He was a Senior Research Fellow in the Department of Applied Physics, Caltech, before joining the National Tsing Hua University, Hsinchu, Taiwan, as an Associate Professor of physics in 1995. In 1998, he joined Jet Propulsion Laboratory, Caltech, and is currently a Senior Member of Engineering Staff in the Device Research and Applications Section. His research activities include the theoretical studies of electronic and optical properties of semiconductor alloys, quantum wells, and superlattices, modeling of heterostructure infrared detectors and lasers, quantum transport in tunnel devices and nanostructure, and optical simulations. Results of his research have been reported in over 80 research publications and in many technical presentations.

Dr. Ting is a member of the American Physical Society, IEEE Lasers and Electro-Optics Society, and the Materials Research Society.

E. M. Luong, photograph and biography not available at the time of publication.

J. D. Vincent, photograph and biography not available at the time of publication.

Craig A. Shott received the B.S. degree from the University of California, Santa Cruz, in 1985. He pursued graduate-level coursework in solid state electrical engineering at the University of California, Santa Barbara, while working at Santa Barbara Research Center.

Since 1989, he has been with the Amber Engineering, a Raytheon Company, Goleta, CA, where he is currently Manager of Advanced Processes, and has developed processes for HgCdTe, InSb, GaAs QWIP, and SiGe FPA devices. His most recent work involves developing processes for uncooled microbolometer device fabrication.

Jason M. Mumolo is currently pursuing the B.S. degree in electrical engineering at Cal Poly Pomona University, Pomona, CA. He has been interning with the QWIP group, Jet Propulsion Laboratory, California Institute of Technology, Pasadena, since early 1997, aiding in infrared device testing and characterization. He plans to pursue the M.S. degree in telecommunications.

J. Long, photograph and biography not available at the time of publication.

Paul D. LeVan received the M. S. and Ph.D. degrees in physics from the University of California, San Diego, in 1978 and 1982, respectively.

He has been with the Air Force Research Laboratory, and its precursory organizations, for the last 18 years. His areas of specialty include infrared focal plane arrays and the levels of system performance enabled by them, as constrained by the background levels against which the system operates.

Nhan Q. Tran is currently pursuing the B.S. degree in electrical engineering at Cal Poly Pomona University, Pomona, CA. He has been interning with the QWIP group, at Jet Propulsion Laboratory, California Institute of Technology, Pasadena, since early 1998, aiding in infrared device testing and characterization. He plans to pursue the M.S. degree in telecommunications.